Rotor Flux and Speed Observers for Induction Motors

Chunki Kwon, Scott D. Sudhoff,
and Stanislaw H. Żak
School of Electrical and Computer Engineering
Purdue University
West Lafayette, IN 47907, USA

Stefen Hui
Department of Mathematical Sciences,
San Diego State University
San Diego, CA 92182, USA

***Abstract*— The objective of this paper is to investigate the use of observers in the sensorless control of induction motor drives. First, three recently proposed rotor flux and speed observers for induction motors are analyzed and compared using a unified notation. Unresolved issues for each method are noted. Then, an alternative rotor flux and speed observer architecture is described, which is simulated and tested experimentally. The conclusion of our study is that observers can perform well estimating the rotor speed and the estimates can be used in a control strategy instead of speed values obtained by the sensors.**

I. Introduction

An observer is an auxiliary dynamical system that uses the plant's input and output signals to generate an estimate of the plant's state, which can then be employed to close the control loop. An observer can also be used to augment or replace sensors in a control system. Effective control strategies of induction motor drive systems require speed as well as the flux estimates. In this paper, we analyze and compare four different rotor flux and speed observers for induction motors using a unified notation. We first review the three recently proposed rotor flux and speed observers for induction motors and then describe an alternative rotor flux and speed observer architecture for an induction motor. We first analyze the adaptive flux observer of Kubota, Matsuse and Nakano [1], where Luenberger's full-order observer is utilized to estimate the stator currents and rotor fluxes using the fourth-order portion of the fifth-order induction motor model in the stationary reference frame and assuming constant rotor speed. Then, a proportional-plus-integral formula is employed to implement the proposed scheme for speed estimation. The above architecture was also analyzed and tested in [2]. Next, we analyze the architecture of Derdiyok et al. [3], where the output of a sliding-mode observer is used in the formula for the flux to obtain an estimate of the rotor flux. We then compare the above two architectures with the rotor flux and speed sliding mode observer proposed by Utkin, Guldner and Shi [4], which is also based on the fourth-order portion of the fifth-order induction motor model in the stationary reference frame and assuming the constant rotor speed. We do not discuss in this paper the Verghese and Sanders' flux observer [5] where the authors focus on estimating the rotor flux only. For further discussion concerning the role the observers play in sensorless control of induction motors the reader may consult [6]. We then proceed with the development of an alternative observer for rotor flux and speed. We represent the standard model of the induction motor in the form

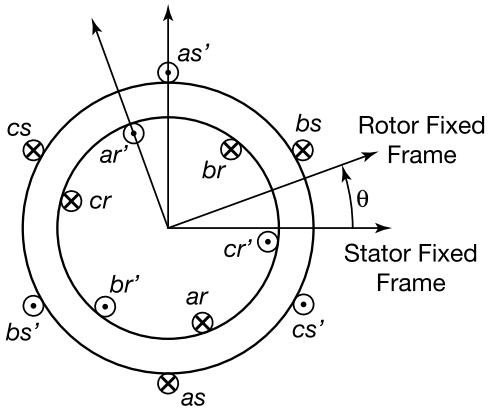

Fig. 1. A 2-pole, 3-phase, smooth air-gap, cage induction motor.

$$\dot{\boldsymbol{x}} = \boldsymbol{A}\boldsymbol{x} + \boldsymbol{B}_1\boldsymbol{u}_1 + \boldsymbol{B}_2\boldsymbol{u}_2(\boldsymbol{x}, \tau_L),$$

where the vector function $\boldsymbol{u}_2$ models lumped nonlinearities in the model and τ_l is the load torque. The dynamics of the proposed observer are described by

$$\dot{\hat{\boldsymbol{x}}} = \boldsymbol{A}\hat{\boldsymbol{x}} + \boldsymbol{B}_1\boldsymbol{u}_1 + \boldsymbol{B}_2\boldsymbol{u}_2(\hat{\boldsymbol{x}}, \hat{\tau}_L),$$

where $\hat{\boldsymbol{x}}$ is the state estimate and $\hat{\tau}_L$ is the load torque estimate.

II. Induction Motor Modeling

A three-pole three-phase smooth air gap induction machine is shown in Figure 1. We use an equivalent two-phase two-pole representation shown in Figure 2. Definitions of state and control variables are given in Table I. Parameters that appear in the modeling equations are given in Table II. We first write the voltage equations for the 2-phase symmetrical smooth air-gap

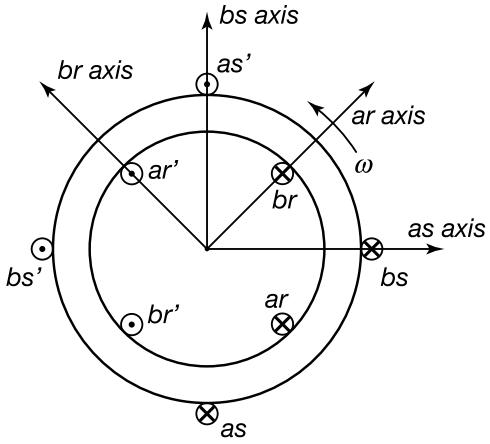

Fig. 2. Converting from 3-phase to a 2-phase equivalent representation.

TABLE I

STATE VARIABLES USED IN THE MODELING OF THE INDUCTION MOTOR.

ω	rotor angular speed
λ_{ar}	rotor flux linkage of phase a
λ_{br}	rotor flux linkage of phase b
i_{as}	stator current in phase a
i_{bs}	stator current in phase b
u_{as}	stator voltage of phase a
u_{bs}	stator voltage of phase b
τ_L	load torque

cage induction motor model:

$$\begin{aligned} u_{as} &= R_s i_{as} + \frac{d\psi_{as}}{dt} \\ u_{bs} &= R_s i_{bs} + \frac{d\psi_{bs}}{dt} \\ 0 &= R_r i_{ar} + \frac{d\psi_{ar}}{dt} \\ 0 &= R_r i_{br} + \frac{d\psi_{br}}{dt}. \end{aligned}$$

We assume that the magnetic system is linear and therefore the flux linkages may be expressed as linear functions of inductances and currents. The stator and rotor windings are in relative motion. When the magnetic axes are aligned, the magnetic coupling between the corresponding windings is maximized and the corresponding mutual inductance is positive and maximized. When the magnetic axes are perpendicular, the magnetic coupling is zero and the mutual inductance value is zero. Taking the above into account, we obtain

$$\begin{aligned} u_{as} &= R_s i_{as} + \frac{d\psi_{as}}{dt} = R_s i_{as} + L_s \frac{di_{as}}{dt} \\ &\quad + L_m \frac{d}{dt}(i_{ar}\cos(n_p\theta) - i_{br}\sin(n_p\theta)) \\ u_{bs} &= R_s i_{bs} + \frac{d\psi_{bs}}{dt} = R_s i_{bs} + L_s \frac{di_{bs}}{dt} \\ &\quad + L_m \frac{d}{dt}(i_{ar}\sin(n_p\theta) + i_{br}\cos(n_p\theta)) \\ 0 &= R_r i_{ar} + \frac{d\psi_{ar}}{dt} = R_r i_{ar} + L_r \frac{di_{ar}}{dt} \\ &\quad + L_m \frac{d}{dt}(i_{as}\cos(n_p\theta) + i_{bs}\sin(n_p\theta)) \\ 0 &= R_r i_{br} + \frac{d\psi_{br}}{dt} = R_r i_{ar} + L_r \frac{di_{ar}}{dt} \\ &\quad + L_m \frac{d}{dt}(-i_{as}\sin(n_p\theta) + i_{bs}\cos(n_p\theta)) \\ J\frac{d\omega}{dt} &= n_p L_m \left(i_{bs}\left(i_{ar}\cos(n_p\theta) - i_{ar}\sin(n_p\theta)\right)\right. \\ &\quad \left. - i_{as}\left(i_{ar}\sin(n_p\theta) + i_{br}\cos(n_p\theta)\right)\right) \\ &\quad - D\omega - \tau_L. \end{aligned}$$

We next apply a model simplifying transformation of the 2-phase equivalent model. Specifically, we use the equivalent set of rotor flux linkages

$$\begin{bmatrix} \lambda_{ar} \\ \lambda_{br} \end{bmatrix} = \begin{bmatrix} \cos(n_p\theta) & -\sin(n_p\theta) \\ \sin(n_p\theta) & \cos(n_p\theta) \end{bmatrix} \begin{bmatrix} \psi_{ar} \\ \psi_{br} \end{bmatrix}$$

to obtain

$$\begin{aligned} \lambda_{ar} &= L_r(i_{ar}\cos(np\theta) - i_{br}\sin(n_p\theta)) + L_m i_{as} \\ \lambda_{br} &= L_r(i_{ar}\sin(np\theta) + i_{br}\cos(n_p\theta)) + L_m i_{bs}. \end{aligned}$$

After some manipulations, we can represent the two-phase equivalent model of a three-phase cage induction motor in the form:

$$\left.\begin{array}{rcl} \frac{d\omega}{dt} &=& \mu(\lambda_{ar} i_{bs} - \lambda_{br} i_{as}) - \frac{D}{J}\omega - \frac{\tau_L}{J} \\ \frac{d\lambda_{ar}}{dt} &=& -\eta\lambda_{ar} - n_p\omega\lambda_{br} + \eta L_m i_{as} \\ \frac{d\lambda_{br}}{dt} &=& -\eta\lambda_{br} + n_p\omega\lambda_{ar} + \eta L_m i_{bs} \\ \frac{di_{as}}{dt} &=& \eta\beta\lambda_{ar} + n_p\beta\omega\lambda_{br} - \gamma i_{as} + \frac{1}{\sigma L_s}u_{as} \\ \frac{di_{bs}}{dt} &=& \eta\beta\lambda_{br} - n_p\beta\omega\lambda_{ar} - \gamma i_{bs} + \frac{1}{\sigma L_s}u_{bs} \end{array}\right\} \quad (1)$$

The above is the cage induction motor model in the stationary reference frame. We illustrate the above modeling equations in Figure 3.

TABLE II

PARAMETERS THAT APPEAR IN THE MODEL OF THE INDUCTION MOTOR.

R_r, R_s	resistance of the rotor, respectively, stator windings
L_r, L_s	self-inductance of the rotor, respectively, stator windings
L_m	mutual inductance of the rotor and stator windings
n_p	number of the pole pairs
D	viscous friction coefficient
η	$= \frac{R_r}{L_r}$
$\sigma = 1 - \frac{L_m^2}{L_r L_s}$	leakage parameter
β	$= \frac{L_m}{\sigma L_r L_s}$
μ	$= \frac{3}{2}\frac{n_p L_m}{J L_r}$
γ	$= \frac{1}{\sigma L_s}\left(R_s + \frac{L_m^2}{L_r^2}R_r\right)$

III. KUBOTA, MATSUSE AND NAKANO'S ADAPTIVE FLUX AND SPEED OBSERVER

Kubota, Matsuse and Nakano [1] use the following fourth-order portion of model (1) when constructing their observer,

$$\begin{bmatrix} \frac{d\lambda_{ar}}{dt} \\ \frac{d\lambda_{br}}{dt} \\ \frac{di_{as}}{dt} \\ \frac{di_{bs}}{dt} \end{bmatrix} = \left[\begin{array}{cc|cc} -\eta & -n_p\omega & \eta L_m & 0 \\ n_p\omega & -\eta & 0 & \eta L_m \\ \hline \eta\beta & n_p\beta\omega & -\gamma & 0 \\ -n_p\beta\omega & \eta\beta & 0 & -\gamma \end{array}\right] \begin{bmatrix} \lambda_{ar} \\ \lambda_{br} \\ i_{as} \\ i_{bs} \end{bmatrix}$$

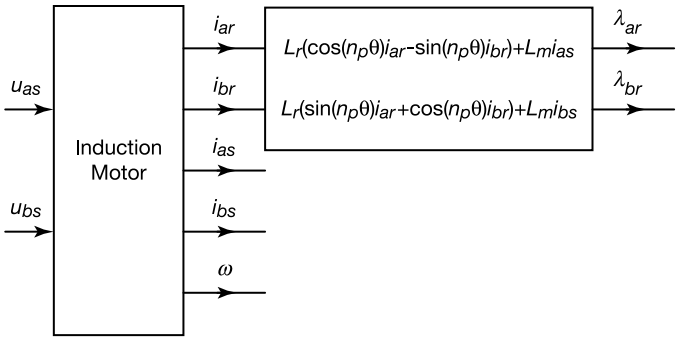

Fig. 3. Induction motor drive two-phase equivalent model schematic.

$$
\begin{aligned}
&+\left[\begin{array}{cc|cc} 0 & 0 & & \\ 0 & 0 & & \\ \hline \frac{1}{\sigma L_s} & 0 & & \\ 0 & \frac{1}{\sigma L_s} & & \end{array}\right]\left[\begin{array}{c} u_{as} \\ u_{bs} \end{array}\right] \\
&= \boldsymbol{A}_r\boldsymbol{x}+\boldsymbol{B}_r\boldsymbol{u}_s, \\
\boldsymbol{y} &= \left[\begin{array}{cc|cc} 0 & 0 & 1 & 0 \\ 0 & 0 & 0 & 1 \end{array}\right]\boldsymbol{x} \\
&= \boldsymbol{C}_r\boldsymbol{x},
\end{aligned}
$$

where the subscript 'r' is used to indicate the reduced-order model. We rearranged the order of modeling equations that Kubota et al. [1] use for the sake of uniformity of our discussion in this paper. Using the above model, Kubota et al. [1] construct the Luenberger full-order observer of the form

$$\frac{d}{dt}\hat{\boldsymbol{x}} = \hat{\boldsymbol{A}}_r\hat{\boldsymbol{x}}+\boldsymbol{B}_r\boldsymbol{u}_s+\boldsymbol{L}_r(\boldsymbol{i}_s-\hat{\boldsymbol{i}}_s),$$

where the symbol $\hat{\boldsymbol{A}}_r$, rather than $\boldsymbol{A}_r$, is used in the observer to denote that an estimated value of ω is utilized. Let

$$\Delta\omega = \hat{\omega}-\omega \;\text{ and }\; \Delta\boldsymbol{A}_r = \hat{\boldsymbol{A}}_r-\boldsymbol{A}_r.$$

Then

$$
\begin{aligned}
\Delta\boldsymbol{A}_r &= \left[\begin{array}{cccc} -\eta & -n_p\hat{\omega} & \eta L_m & 0 \\ n_p\hat{\omega} & -\eta & 0 & \eta L_m \\ \eta\beta & n_p\beta\hat{\omega} & -\gamma & 0 \\ -n_p\beta\hat{\omega} & \eta\beta & 0 & -\gamma \end{array}\right] \\
&\quad -\left[\begin{array}{cccc} -\eta & -n_p\omega & \eta L_m & 0 \\ n_p\omega & -\eta & 0 & \eta L_m \\ \eta\beta & n_p\beta\omega & -\gamma & 0 \\ -n_p\beta\omega & \eta\beta & 0 & -\gamma \end{array}\right] \\
&= \left[\begin{array}{cccc} 0 & -n_p\Delta\omega & 0 & 0 \\ n_p\Delta\omega & 0 & 0 & 0 \\ 0 & n_p\beta\Delta\omega & 0 & 0 \\ -n_p\beta\Delta\omega & 0 & 0 & 0 \end{array}\right].
\end{aligned}
$$

Let $\boldsymbol{e} = \boldsymbol{x}-\hat{\boldsymbol{x}}$, then it follows from $\hat{\boldsymbol{A}}_r = \boldsymbol{A}_r+\Delta\boldsymbol{A}_r$ that

$$
\begin{aligned}
\frac{d}{dt}\boldsymbol{e} &= \boldsymbol{A}_r\boldsymbol{x}+\boldsymbol{B}\boldsymbol{u}_s-\hat{\boldsymbol{A}}_r\hat{\boldsymbol{x}}-\boldsymbol{B}_r\boldsymbol{u}_s-\boldsymbol{L}_r(\boldsymbol{y}-\hat{\boldsymbol{y}}) \\
&= \boldsymbol{A}_r\boldsymbol{x}-\boldsymbol{A}_r\hat{\boldsymbol{x}}-\Delta\boldsymbol{A}_r\hat{\boldsymbol{x}}-\boldsymbol{L}_r\boldsymbol{C}_r(\boldsymbol{x}-\hat{\boldsymbol{x}}) \\
&= (\boldsymbol{A}_r-\boldsymbol{L}_r\boldsymbol{C}_r)\boldsymbol{e}-\Delta\boldsymbol{A}_r\hat{\boldsymbol{x}}. \qquad (2)
\end{aligned}
$$

Kubota et al. [1] next postulate selecting $\boldsymbol{L}_r$ so that

$$(\boldsymbol{A}_r-\boldsymbol{L}_r\boldsymbol{C}_r)^T+(\boldsymbol{A}_r-\boldsymbol{L}_r\boldsymbol{C}_r)<0, \qquad (3)$$

which amounts to finding an observer gain matrix $\boldsymbol{L}_r$ so that $V(\boldsymbol{e}) = \boldsymbol{e}^T\boldsymbol{e}$ is a Lyapunov function for the system $\dot{\boldsymbol{e}} = (\boldsymbol{A}_r-\boldsymbol{L}_r\boldsymbol{C}_r)\boldsymbol{e}$, that is,

$$(\boldsymbol{A}_r-\boldsymbol{L}_r\boldsymbol{C}_r)^T+(\boldsymbol{A}_r-\boldsymbol{L}_r\boldsymbol{C}_r) = -\boldsymbol{Q},$$

where $\boldsymbol{Q} = \boldsymbol{Q}^T > 0$. The above requirement greatly simplifies further analysis; however, sufficiency conditions for the existence of the gain matrix $\boldsymbol{L}_r$ such that (3) is satisfied is not discussed in their paper and appears to be unknown in the iterature. Kubota et al. [1] then consider an augmented Lyapunov's function candidate:

$$V(\boldsymbol{e},\Delta\omega) = \boldsymbol{e}^T\boldsymbol{e}+\frac{1}{\alpha}(\hat{\omega}-\omega)^2,$$

where $\alpha > 0$ is a design parameter. Recall that $\Delta\omega = \hat{\omega}-\omega$. In their further development Kubota et al. [1] assume that ω is constant. Then, evaluating the time derivative of $V(\boldsymbol{e},\Delta\omega)$ on the trajectories of (2) gives

$$
\begin{aligned}
\frac{d}{dt}V(\boldsymbol{e},\Delta\omega) &= \frac{d}{dt}\left(\boldsymbol{e}^T\boldsymbol{e}+\frac{1}{\alpha}(\Delta\omega)^2\right) \\
&= 2\boldsymbol{e}^T\dot{\boldsymbol{e}}+\frac{2}{\alpha}\Delta\omega\frac{d}{dt}\Delta\omega \\
&= 2\boldsymbol{e}^T\left((\boldsymbol{A}_r-\boldsymbol{L}_r\boldsymbol{C}_r)\boldsymbol{e}-\Delta\boldsymbol{A}_r\hat{\boldsymbol{x}}\right) \\
&\quad +\frac{2}{\alpha}\Delta\omega\frac{d}{dt}\hat{\omega} \\
&= -\boldsymbol{e}^T\boldsymbol{Q}\boldsymbol{e}-2\boldsymbol{e}^T\Delta\boldsymbol{A}_r\hat{\boldsymbol{x}} \\
&\quad +\frac{2}{\alpha}\Delta\omega\frac{d}{dt}\hat{\omega}. \qquad (4)
\end{aligned}
$$

To proceed, we need to evaluate

$$
\begin{aligned}
&\boldsymbol{e}^T\Delta\boldsymbol{A}_r\hat{\boldsymbol{x}} \\
&= \left[\begin{array}{cccc} \lambda_{ar}-\hat{\lambda}_{ar} & \lambda_{br}-\hat{\lambda}_{br} & i_{as}-\hat{i}_{as} & i_{bs}-\hat{i}_{bs} \end{array}\right] \\
&\quad \times\left[\begin{array}{cccc} 0 & -n_p\Delta\omega & 0 & 0 \\ n_p\Delta\omega & 0 & 0 & 0 \\ 0 & n_p\beta\Delta\omega & 0 & 0 \\ -n_p\beta\Delta\omega & 0 & 0 & 0 \end{array}\right]\left[\begin{array}{c} \hat{\lambda}_{ar} \\ \hat{\lambda}_{br} \\ \hat{i}_{as} \\ \hat{i}_{bs} \end{array}\right] \\
&= \left[\begin{array}{c} \lambda_{ar}-\hat{\lambda}_{ar} \\ \lambda_{br}-\hat{\lambda}_{br} \\ i_{as}-\hat{i}_{as} \\ i_{bs}-\hat{i}_{bs} \end{array}\right]^T\times\left[\begin{array}{c} -n_p\Delta\omega\hat{\lambda}_{br} \\ n_p\Delta\omega\hat{\lambda}_{ar} \\ n_p\beta\Delta\omega\hat{\lambda}_{br} \\ -n_p\beta\Delta\omega\hat{\lambda}_{ar} \end{array}\right] \\
&= \Delta\omega\Big(-\left(\lambda_{ar}-\hat{\lambda}_{ar}\right)n_p\hat{\lambda}_{br} \\
&\quad +\left(\lambda_{br}-\hat{\lambda}_{br}\right)n_p\hat{\lambda}_{ar}+(i_{as}-\hat{i}_{as})n_p\beta\hat{\lambda}_{br} \\
&\quad -(i_{bs}-\hat{i}_{bs})n_p\beta\hat{\lambda}_{ar}\Big) \\
&= \Delta\omega\Big(-\lambda_{ar}n_p\hat{\lambda}_{br}+\hat{\lambda}_{ar}n_p\hat{\lambda}_{br}+\lambda_{br}n_p\hat{\lambda}_{ar} \\
&\quad -\hat{\lambda}_{br}n_p\hat{\lambda}_{ar}+(i_{as}-\hat{i}_{as})n_p\beta\hat{\lambda}_{br} \\
&\quad -(i_{bs}-\hat{i}_{bs})n_p\beta\hat{\lambda}_{ar}\Big).
\end{aligned}
$$

Kubota et al. [1] assume, without stating this explicitly, that

$$\lambda_{ar} n_p \hat{\lambda}_{br} = \lambda_{br} n_p \hat{\lambda}_{ar},$$

that is,

$$\lambda_{ar} \hat{\lambda}_{br} = \hat{\lambda}_{ar} \lambda_{br}. \tag{5}$$

Taking the above into account in the expression for $\boldsymbol{e}^T \Delta \boldsymbol{A}_r \hat{\boldsymbol{x}}$ yields

$$\boldsymbol{e}^T \Delta \boldsymbol{A}_r \hat{\boldsymbol{x}} = \Delta\omega (i_{as} - \hat{i}_{as}) n_p \beta \hat{\lambda}_{br} - (i_{bs} - \hat{i}_{bs}) n_p \beta \hat{\lambda}_{ar}.$$

Substituting the above into (4) gives

$$\begin{aligned} &\frac{d}{dt} V(\boldsymbol{e}, \Delta\omega) \\ &= -\boldsymbol{e}^T \boldsymbol{Q} \boldsymbol{e} - 2\Delta\omega \left((i_{as} - \hat{i}_{as}) n_p \beta \hat{\lambda}_{br} \right. \\ &\quad \left. - (i_{bs} - \hat{i}_{bs}) n_p \beta \hat{\lambda}_{ar} \right) + \frac{2}{\alpha} \Delta\omega \frac{d}{dt} \hat{\omega} \\ &= -\boldsymbol{e}^T \boldsymbol{Q} \boldsymbol{e} + 2\Delta\omega \left(\frac{1}{\alpha} \frac{d}{dt} \hat{\omega} - \left((i_{as} - \hat{i}_{as}) n_p \beta \hat{\lambda}_{br} \right. \right. \\ &\quad \left. \left. - (i_{bs} - \hat{i}_{bs}) n_p \beta \hat{\lambda}_{ar} \right) \right). \end{aligned}$$

If we let

$$\frac{d}{dt} \hat{\omega} = \alpha \left((i_{as} - \hat{i}_{as}) n_p \beta \hat{\lambda}_{br} - (i_{bs} - \hat{i}_{bs}) n_p \beta \hat{\lambda}_{ar} \right),$$

then $\frac{d}{dt} V(\boldsymbol{e}, \Delta\omega) = -\boldsymbol{e}^T \boldsymbol{Q} \boldsymbol{e} \leq 0$ in the augmented $\begin{bmatrix} \boldsymbol{e} \\ \Delta\omega \end{bmatrix}$-space. Recall that the adaptive scheme was obtained under the assumption that ω is constant. Kubota et al. [1] propose to use the PI control to implement the above scheme,

$$\begin{aligned} \hat{\omega} &= K_P \left((i_{as} - \hat{i}_{as}) n_p \beta \hat{\lambda}_{br} - (i_{bs} - \hat{i}_{bs}) n_p \beta \hat{\lambda}_{ar} \right) \\ &+ K_I \int \left((i_{as} - \hat{i}_{as}) n_p \beta \hat{\lambda}_{br} - (i_{bs} - \hat{i}_{bs}) n_p \beta \hat{\lambda}_{ar} \right) dt. \end{aligned}$$

In summary, the observer of Kubota, Matsuse, and Nakano [1] has the form,

$$\begin{aligned} &\frac{d}{dt} \begin{bmatrix} \hat{\lambda}_{ar} \\ \hat{\lambda}_{br} \\ \hat{i}_{as} \\ \hat{i}_{bs} \end{bmatrix} \\ &= \left[\begin{array}{cc|cc} -\eta & -n_p \hat{\omega} & \eta L_m & 0 \\ n_p \hat{\omega} & -\eta & 0 & \eta L_m \\ \hline \eta\beta & n_p \beta \hat{\omega} & -\gamma & 0 \\ -n_p \beta \hat{\omega} & \eta\beta & 0 & -\gamma \end{array} \right] \begin{bmatrix} \hat{\lambda}_{ar} \\ \hat{\lambda}_{br} \\ \hat{i}_{as} \\ \hat{i}_{bs} \end{bmatrix} \\ &+ \left[\begin{array}{cc} 0 & 0 \\ 0 & 0 \\ \hline \frac{1}{\sigma L_s} & 0 \\ 0 & \frac{1}{\sigma L_s} \end{array} \right] \begin{bmatrix} u_{as} \\ u_{bs} \end{bmatrix} + \boldsymbol{L}_r \left(\begin{bmatrix} \hat{i}_{as} - i_{as} \\ \hat{i}_{bs} - i_{bs} \end{bmatrix} \right) \\ \hat{\omega} &= K_P \left((i_{as} - \hat{i}_{as}) n_p \beta \hat{\lambda}_{br} - (i_{bs} - \hat{i}_{bs}) n_p \beta \hat{\lambda}_{ar} \right) \\ &+ K_I \int \left((i_{as} - \hat{i}_{as}) n_p \beta \hat{\lambda}_{br} - (i_{bs} - \hat{i}_{bs}) n_p \beta \hat{\lambda}_{ar} \right) dt. \end{aligned}$$

IV. Sliding Mode Observer of Derdiyok, Güven, Rehman, Inanc and Xu

As in the observer of Kubota et al., Derdiyok et al. [3] use the fourth-order portion of the fifth-order induction motor model in the stationary reference frame. We now describe the representation of the model that Derdiyok et al. [3] use when constructing their observer. Let

$$\boldsymbol{A}_\omega = \begin{bmatrix} \eta & n_p \omega \\ -n_p \omega & \eta \end{bmatrix}.$$

Then we can represent the reduced-order model as:

$$\frac{d\boldsymbol{\lambda}_r}{dt} = -\boldsymbol{A}_\omega \boldsymbol{\lambda}_r + \eta L_m \boldsymbol{i}_s \tag{6}$$

$$\frac{d\boldsymbol{i}_s}{dt} = \beta \boldsymbol{A}_\omega \boldsymbol{\lambda}_r - \gamma \boldsymbol{i}_s + \frac{1}{\sigma L_s} \boldsymbol{u}_s. \tag{7}$$

The following switching surface is defined,

$$\boldsymbol{s} = \begin{bmatrix} s_a \\ s_b \end{bmatrix} = \begin{bmatrix} \hat{i}_{as} - i_{as} \\ \hat{i}_{bs} - i_{bs} \end{bmatrix} = \boldsymbol{0}.$$

Let

$$\boldsymbol{\nu} = -\nu_0 \begin{bmatrix} \text{sign}(s_a) \\ \text{sign}(s_b) \end{bmatrix} = -\nu_0 \begin{bmatrix} \text{sign}(\hat{i}_{as} - i_{as}) \\ \text{sign}(\hat{i}_{bs} - i_{bs}) \end{bmatrix}.$$

Derdiyok et al. [3] propose the current observer:

$$\frac{d\hat{\boldsymbol{i}}_s}{dt} = \beta \boldsymbol{\nu} - \gamma \hat{\boldsymbol{i}}_s + \frac{1}{\sigma L_s} \boldsymbol{u}_s. \tag{8}$$

We now use the arguments of Derdiyok et al. [3] to show that the surface $\{\boldsymbol{s} = \boldsymbol{0}\}$ is attractive for sufficiently large gain ν_0. For this we consider a generalized Lyapunov function candidate, $V = 0.5 \boldsymbol{s}^T \boldsymbol{s}$, which can be viewed as a distance measure from $\{\boldsymbol{s} = \boldsymbol{0}\}$, We then find the Lyapunov derivative of V, that is, the time derivative of V evaluated on the trajectories of the observer, $\dot{V} = \boldsymbol{s}^T \dot{\boldsymbol{s}}$, where

$$\begin{aligned} \dot{\boldsymbol{s}} &= \frac{d}{dt} \hat{\boldsymbol{i}}_s - \frac{d}{dt} \boldsymbol{i}_s \\ &= \beta \boldsymbol{\nu} - \gamma \hat{\boldsymbol{i}}_s + \frac{1}{\sigma L_s} \boldsymbol{v}_s - \beta \boldsymbol{A}_\omega \boldsymbol{\lambda}_r + \gamma \boldsymbol{i}_s - \frac{1}{\sigma L_s} \boldsymbol{v}_s \\ &= \beta \left(\boldsymbol{\nu} - \beta \boldsymbol{A}_\omega \boldsymbol{\lambda}_r \right) - \gamma \left(\hat{\boldsymbol{i}}_s - \boldsymbol{i}_s \right). \end{aligned}$$

Let

$$\textbf{sign}(\boldsymbol{x}) = \begin{bmatrix} \text{sign}(x_1) & \text{sign}(x_2) & \cdots & \text{sign}(x_n) \end{bmatrix}^T.$$

Then

$$\begin{aligned} \dot{V} &= \beta \left(\hat{\boldsymbol{i}}_s - \boldsymbol{i}_s \right)^T \left(\boldsymbol{\nu} - \beta \boldsymbol{A}_\omega \boldsymbol{\lambda}_r \right) - \gamma \left\| \hat{\boldsymbol{i}}_s - \boldsymbol{i}_s \right\|^2 \\ &= -\beta \nu_0 \left(\hat{\boldsymbol{i}}_s - \boldsymbol{i}_s \right)^T \textbf{sign} \left(\hat{\boldsymbol{i}}_s - \boldsymbol{i}_s \right) - \gamma \left\| \hat{\boldsymbol{i}}_s - \boldsymbol{i}_s \right\|^2 \\ &\quad - \beta^2 \left(\hat{\boldsymbol{i}}_s - \boldsymbol{i}_s \right)^T \boldsymbol{A}_\omega \boldsymbol{\lambda}_r \\ &= -\beta \nu_0 \left(\left| \hat{i}_{sa} - i_{sa} \right| + \left| \hat{i}_{sb} - i_{sb} \right| \right) - \gamma \left\| \hat{\boldsymbol{i}}_s - \boldsymbol{i}_s \right\|^2 \\ &\quad - \beta^2 \left(\hat{\boldsymbol{i}}_s - \boldsymbol{i}_s \right)^T \boldsymbol{A}_\omega \boldsymbol{\lambda}_r. \end{aligned}$$

Note that $\beta > 0$. Thus $\dot{V} < 0$ if

$$\nu_0 \left(\left| \hat{i}_{sa} - i_{sa} \right| + \left| \hat{i}_{sb} - i_{sb} \right| \right) > -\frac{\gamma}{\beta} \left\| \hat{\boldsymbol{i}}_s - \boldsymbol{i}_s \right\|^2 - \beta \left(\hat{\boldsymbol{i}}_s - \boldsymbol{i}_s \right)^T \boldsymbol{A}_\omega \boldsymbol{\lambda}_r.$$

Therefore, $\dot{V} < 0$ if

$$\nu_0 > \frac{\beta \left| \left(\hat{\boldsymbol{i}}_s - \boldsymbol{i}_s \right)^T \boldsymbol{A}_\omega \boldsymbol{\lambda}_r \right| - \frac{\gamma}{\beta} \left\| \hat{\boldsymbol{i}}_s - \boldsymbol{i}_s \right\|^2}{\left| \hat{i}_{sa} - i_{sa} \right| + \left| \hat{i}_{sb} - i_{sb} \right|}.$$

The above condition requires careful analysis. Note that for the system in sliding the denominator of the term on the right-hand side of the above condition is 0 and the fraction is not defined. Derdiyok et al. [3] do not discuss this issue in their paper. We analyze the situation as follows. The key is that, in practice, the denominator is small and not identically 0 in sliding and we must be careful that the fraction does not become unbounded as the denominator tends to 0. We analyze the terms in the numerator separately. If $\left| \hat{i}_{sa} - i_{sa} \right| + \left| \hat{i}_{sb} - i_{sb} \right| < 1$, then

$$\left\| \hat{\boldsymbol{i}}_s - \boldsymbol{i}_s \right\|^2 \leq \left\| \hat{\boldsymbol{i}}_s - \boldsymbol{i}_s \right\| \leq \left| \hat{i}_{sa} - i_{sa} \right| + \left| \hat{i}_{sb} - i_{sb} \right|.$$

It follows that if $0 < \left| \hat{i}_{sa} - i_{sa} \right| + \left| \hat{i}_{sb} - i_{sb} \right| < 1$, then

$$\frac{\left\| \hat{\boldsymbol{i}}_s - \boldsymbol{i}_s \right\|^2}{\left| \hat{i}_{sa} - i_{sa} \right| + \left| \hat{i}_{sb} - i_{sb} \right|} \leq 1.$$

We next analyze the other term is the numerator. Recall that $\boldsymbol{A}_\omega \boldsymbol{\lambda}_r = \begin{bmatrix} \nu_1 & \nu_2 \end{bmatrix}^T$. Hence,

$$\begin{aligned} &\left| \left(\hat{\boldsymbol{i}}_s - \boldsymbol{i}_s \right)^T \boldsymbol{A}_\omega \boldsymbol{\lambda}_r \right| \\ &\quad \leq \left| \hat{i}_{sa} - i_{sa} \right| |\nu_1| + \left| \hat{i}_{sb} - i_{sb} \right| |\nu_2| \\ &\quad \leq \max\{|\nu_1|, |\nu_2|\} \left(\left| \hat{i}_{sa} - i_{sa} \right| + \left| \hat{i}_{sb} - i_{sb} \right| \right). \end{aligned}$$

The above inequalities give, for $0 < \left| \hat{i}_{sa} - i_{sa} \right| + \left| \hat{i}_{sb} - i_{sb} \right| < 1$,

$$\frac{\beta \left| \left(\hat{\boldsymbol{i}}_s - \boldsymbol{i}_s \right)^T \boldsymbol{A}_\omega \boldsymbol{\lambda}_r \right| - \frac{\gamma}{\beta} \left\| \hat{\boldsymbol{i}}_s - \boldsymbol{i}_s \right\|^2}{\left| \hat{i}_{sa} - i_{sa} \right| + \left| \hat{i}_{sb} - i_{sb} \right|} \leq \beta \max\{|\nu_1|, |\nu_2|\} + \frac{\gamma}{\beta}.$$

We conclude that the fraction is bounded for practical purposes.

When the observation error is in sliding mode along the surface $\{\boldsymbol{s} = \boldsymbol{0}\}$, we have

$$\hat{\boldsymbol{i}}_s - \boldsymbol{i}_s = \boldsymbol{0} \text{ and } \frac{d}{dt} \left(\hat{\boldsymbol{i}}_s - \boldsymbol{i}_s \right) = \boldsymbol{0}.$$

It follows from the above conditions applied to (7) and (8) that in sliding, $\boldsymbol{\nu} = \boldsymbol{A}_\omega \boldsymbol{\lambda}_r$. Substituting the above into the modeling equation gives

$$\frac{d}{dt} \boldsymbol{\lambda}_r = -\boldsymbol{\nu} + \eta L_m \boldsymbol{i}_s.$$

We solve the above for $\boldsymbol{\lambda}_r$ and then using $\boldsymbol{\nu} = \boldsymbol{A}_\omega \boldsymbol{\lambda}_r$, we obtain

$$\begin{aligned} \begin{bmatrix} \nu_1 \\ \nu_2 \end{bmatrix} &= \begin{bmatrix} \eta & n_p\omega \\ -n_p\omega & \eta \end{bmatrix} \begin{bmatrix} \lambda_{ar} \\ \lambda_{br} \end{bmatrix} \\ &= \begin{bmatrix} \eta\lambda_{ar} + n_p\omega\lambda_{br} \\ -n_p\omega\lambda_{ar} + \eta\lambda_{br} \end{bmatrix} \\ &= \begin{bmatrix} \lambda_{ar} & \lambda_{br} \\ \lambda_{br} & -\lambda_{ar} \end{bmatrix} \begin{bmatrix} \eta \\ n_p\omega \end{bmatrix}. \end{aligned}$$

Hence

$$\begin{bmatrix} \eta \\ n_p\omega \end{bmatrix} = -\frac{1}{\lambda_{ar}^2 + \lambda_{br}^2} \begin{bmatrix} -\lambda_{ar} & -\lambda_{br} \\ -\lambda_{br} & \lambda_{ar} \end{bmatrix} \begin{bmatrix} \nu_1 \\ \nu_2 \end{bmatrix},$$

that is, we have an estimate of the motor time constant, η, as well as the rotor speed, ω.

V. Sliding Mode Observer of Utkin, Guldner and Shi

Utkin, Guldner and Shi [4] propose a rotor flux and rotor speed observer where they assume that ω is constant when arriving at the proposed observer architecture. To begin with, consider a copy of the induction model subsystem,

$$\begin{aligned} \frac{d\hat{\boldsymbol{\lambda}}_r}{dt} &= -\hat{\boldsymbol{A}}_\omega \hat{\boldsymbol{\lambda}}_r + \eta L_m \hat{\boldsymbol{i}}_s \\ \frac{d\hat{\boldsymbol{i}}_s}{dt} &= \beta \hat{\boldsymbol{A}}_\omega \hat{\boldsymbol{\lambda}}_r - \gamma \hat{\boldsymbol{i}}_s + \frac{1}{\sigma L_s} \boldsymbol{v}_s, \end{aligned}$$

where

$$\hat{\boldsymbol{A}}_\omega = \begin{bmatrix} \eta & n_p\hat{\omega} \\ -n_p\hat{\omega} & \eta \end{bmatrix}.$$

Then, Utkin, Guldner and Shi [4] propose to use as the rotor speed estimate

$$\hat{\omega}_e = \omega_0 \text{sign}(s_n),$$

where

$$s_n = \left(\hat{i}_{bs} - i_{bs} \right) \hat{\lambda}_{ar} - \left(\hat{i}_{as} - i_{as} \right) \hat{\lambda}_{br}$$

and

$$\frac{d}{dt} \begin{bmatrix} \hat{\boldsymbol{\lambda}}_r \\ \hat{\boldsymbol{i}}_s \end{bmatrix} = \begin{bmatrix} -\hat{\boldsymbol{A}}_\omega & \eta L_m \boldsymbol{I}_2 \\ \beta \hat{\boldsymbol{A}}_\omega & -\gamma \boldsymbol{I}_2 \end{bmatrix} \begin{bmatrix} \hat{\boldsymbol{\lambda}}_r \\ \hat{\boldsymbol{i}}_s \end{bmatrix} + \begin{bmatrix} \boldsymbol{O}_{2\times 2} \\ \frac{1}{\sigma L_s} \boldsymbol{I}_2 \end{bmatrix} \boldsymbol{u}_s.$$

Utkin et al. [4, page 225] were not able to provide a proof of the observation error convergence. However, they successfully tested their proposed observer in a laboratory setting.

VI. The Proposed Observer

In this section we use the induction motor model (1) to construct a fifth-order observer. The construction of the proposed observer is inspired by the observer architecture of Thau [7], which is also analyzed in [8], [9]. We add that the Thau observer was generalized by Kou et al. [10] and by

Żak [11], [12]. To proceed, we represent the induction motor model (1) in a form suitable for this observer design,

$$\begin{aligned}
\begin{bmatrix} \frac{d\omega}{dt} \\ \frac{d\lambda_{ar}}{dt} \\ \frac{d\lambda_{br}}{dt} \\ \frac{di_{as}}{dt} \\ \frac{di_{bs}}{dt} \end{bmatrix} &= \begin{bmatrix} -\frac{D}{J} & 0 & 0 & 0 & 0 \\ 0 & -\eta & 0 & \eta L_m & 0 \\ 0 & 0 & -\eta & 0 & \eta L_m \\ 0 & \eta\beta & 0 & -\gamma & 0 \\ 0 & 0 & \eta\beta & 0 & -\gamma \end{bmatrix} \begin{bmatrix} \omega \\ \lambda_{ar} \\ \lambda_{br} \\ i_{as} \\ i_{bs} \end{bmatrix} \\
&\quad + \begin{bmatrix} 0 & 0 \\ 0 & 0 \\ 0 & 0 \\ \frac{1}{\sigma L_s} & 0 \\ 0 & \frac{1}{\sigma L_s} \end{bmatrix} \begin{bmatrix} u_{as} \\ u_{bs} \end{bmatrix} \\
&\quad + \begin{bmatrix} \mu & 0 & 0 \\ 0 & -n_p & 0 \\ 0 & 0 & n_p \\ 0 & n_p\beta & 0 \\ 0 & 0 & -n_p\beta \end{bmatrix} \boldsymbol{u}_2(\boldsymbol{x}, \tau_L) \\
&= \boldsymbol{A}\boldsymbol{x} + \boldsymbol{B}_1\boldsymbol{u}_1 + \boldsymbol{B}_2\boldsymbol{u}_2(\boldsymbol{x}, \tau_L), \qquad (9)
\end{aligned}$$

where

$$\boldsymbol{u}_2(\boldsymbol{x}, \tau_L) = \begin{bmatrix} \lambda_{ar} i_{bs} - \lambda_{br} i_{as} - \frac{1}{\mu J}\tau_L \\ \omega\lambda_{br} \\ \omega\lambda_{ar} \end{bmatrix}.$$

The output equation is

$$\boldsymbol{y} = \begin{bmatrix} 0 & 0 & 0 & 1 & 0 \\ 0 & 0 & 0 & 0 & 1 \end{bmatrix} \begin{bmatrix} \omega \\ \lambda_{ar} \\ \lambda_{br} \\ i_{as} \\ i_{bs} \end{bmatrix} = \boldsymbol{C}\boldsymbol{x}. \qquad (10)$$

Note that the pair $(\boldsymbol{A}, \boldsymbol{C})$ is detectable but not observable. In fact the matrix $\boldsymbol{A}$ has all its eigenvalues in the open left-half complex plane. The designer, however, may decide to shift the observable eigenvalues of $\boldsymbol{A}$ into prespecified locations, that is, the designer may want find a gain matrix $\boldsymbol{L}$ such that the eigenvalues of the matrix $(\boldsymbol{A}-\boldsymbol{L}\boldsymbol{C})$ are as close to prespecified locations in the open left-half complex plane as possible. We assume that the function $\boldsymbol{u}_2$ representing the nonlinearities of the model satisfies a Lipschitz condition with respect to $\boldsymbol{x}$ in some neighborhood of the origin, that is, there exists a positive constant κ such that for any $\boldsymbol{x}$ and $\hat{\boldsymbol{x}}$ in a neighborhood of the origin,

$$\|\boldsymbol{u}_2(\hat{\boldsymbol{x}}, \hat{\tau}_L) - \boldsymbol{u}_2(\boldsymbol{x}, \tau_L)\| \leq \kappa \|\hat{\boldsymbol{x}} - \boldsymbol{x}\|, \qquad (11)$$

where the symbol $\|\cdot\|$ denotes the standard Euclidean norm for vectors and the corresponding induced norm for matrices. The proposed observer has the form

$$\boxed{\dot{\hat{\boldsymbol{x}}} = (\boldsymbol{A} - \boldsymbol{L}\boldsymbol{C})\hat{\boldsymbol{x}} + \boldsymbol{B}_1\boldsymbol{u}_1 + \boldsymbol{L}\boldsymbol{y} + \boldsymbol{B}_2\boldsymbol{u}_2(\hat{\boldsymbol{x}}, \tau_L)} \qquad (12)$$

Let $\boldsymbol{e}(t) = \hat{\boldsymbol{x}}(t) - \boldsymbol{x}(t)$ be the estimation error. The dynamics of the estimation error are governed by the equation,

$$\dot{\boldsymbol{e}}(t) = (\boldsymbol{A} - \boldsymbol{L}\boldsymbol{C})\boldsymbol{e}(t) + \boldsymbol{B}_2\left(\boldsymbol{u}_2(\hat{\boldsymbol{x}}, \hat{\tau}_L) - \boldsymbol{u}_2(\boldsymbol{x}, \tau_L)\right). \qquad (13)$$

Because the matrix $(\boldsymbol{A} - \boldsymbol{L}\boldsymbol{C})$ is asymptotically stable, there exists, for any symmetric positive definite $\boldsymbol{Q}$, a symmetric positive definite $\boldsymbol{P}$ such that

$$(\boldsymbol{A} - \boldsymbol{L}\boldsymbol{C})^T\boldsymbol{P} + \boldsymbol{P}(\boldsymbol{A} - \boldsymbol{L}\boldsymbol{C}) = -\boldsymbol{Q}. \qquad (14)$$

We next consider the positive definite Lyapunov function candidate, $V(\boldsymbol{e}) = \boldsymbol{e}^T\boldsymbol{P}\boldsymbol{e}$, for the error system (13). The time derivative of V evaluated along the solution of (13) is

$$\begin{aligned}
\dot{V}(\boldsymbol{e}) &= 2\boldsymbol{e}^T\boldsymbol{P}\dot{\boldsymbol{e}} \\
&= 2\boldsymbol{e}^T\boldsymbol{P}(\boldsymbol{A} - \boldsymbol{L}\boldsymbol{C})\boldsymbol{e} \\
&\quad + 2\boldsymbol{e}^T\boldsymbol{P}\boldsymbol{B}_2\left(\boldsymbol{u}_2(\hat{\boldsymbol{x}}, \hat{\tau}_L) - \boldsymbol{u}_2(\boldsymbol{x}, \tau_L)\right) \\
&\leq -\boldsymbol{e}^T\boldsymbol{Q}\boldsymbol{e} \\
&\quad + 2\|\boldsymbol{e}\|\|\boldsymbol{B}_2\|\lambda_{\max}(\boldsymbol{P})\|\boldsymbol{u}_2(\hat{\boldsymbol{x}}, \hat{\tau}_L) - \boldsymbol{u}_2(\boldsymbol{x}, \tau_L)\|.
\end{aligned}$$

Taking into account the Lipschitz condition (11), we obtain

$$\begin{aligned}
\dot{V}(\boldsymbol{e}) &\leq -\lambda_{\min}(\boldsymbol{Q})\|\boldsymbol{e}\|^2 + 2\kappa\|\boldsymbol{B}_2\|\lambda_{\max}(\boldsymbol{P})\|\boldsymbol{e}\|^2 \\
&= -\left(\lambda_{\min}(\boldsymbol{Q}) - 2\kappa\|\boldsymbol{B}_2\|\lambda_{\max}(\boldsymbol{P})\right)\|\boldsymbol{e}\|^2.
\end{aligned}$$

Hence if

$$\kappa < \frac{\lambda_{\min}(\boldsymbol{Q})}{2\|\boldsymbol{B}_2\|\lambda_{\max}(\boldsymbol{P})}, \qquad (15)$$

then $\dot{V}(\boldsymbol{e}) < 0$ and $\boldsymbol{e} = \boldsymbol{0}$ is an asymptotically stable equilibrium state of the error equation (12).

We add here that in our implementation of the proposed observer we have $\boldsymbol{L} = \boldsymbol{O}$. To evaluate the upper bound on κ that appears in (15), we used $\boldsymbol{Q} = \boldsymbol{I}_5$, which resulted in $\kappa < 7.5348\times10^{-5}$. Although this upper bound is "very small", the Lipschitz condition (15) is nevertheless satisfied at $t = 0$, that is, at the beginning of the first set of our simulations described in Section IX, where we assume the zero initial conditions for the motor and the observer.

In the next section we describe the induction motor drive that we employ in testing our proposed observer.

VII. Description of the Induction Motor Drive Employed in Simulations and Experiments

The performance of the proposed observer is investigated with computer simulations and laboratory experiments using a 4-pole, 460 V, 50 Hp, 60 Hz, delta-connected induction motor whose specification are listed in Table III. The parameters for the test induction motor are given in Table IV. Substituting

TABLE III
Specification of Baldor ZDM4115T-AM1 induction motor.

Horsepower/Kilowatt	50/37.3
Voltage	230/460
Hertz	60
Phase	3
Full load amps	114/57
RPM	1775
Frame Size	326 TC
Rating	40C AMB-CONT
NEMA Design Code	B
Full Load Efficiency	94.5
Power Factor	87.0
Enclosure	TEBC

TABLE IV

NUMERICAL VALUES OF THE PARAMETERS OF THE INDUCTION MOTOR.

D	0.1 N·m·sec·rad^{-1}
J	0.4203×10^{-4} kg·m^2
L_m	0.0915 H
$L_r = L_s$	0.0957 H
R_r	0.159 Ω
R_s	0.22 Ω
n_p	2

the above parameter values into (9) gives

$$\boldsymbol{A} = \begin{bmatrix} -0.238 & 0 & 0 & 0 & 0 \\ 0 & -11.946 & 0 & 0.109 & 0 \\ 0 & 0 & -11.946 & 0 & 0.109 \\ 0 & 1169.869 & 0 & -42.044 & 0 \\ 0 & 0 & 1169.869 & 0 & -42.044 \end{bmatrix},$$

$$\boldsymbol{B}_1 = \begin{bmatrix} 0 & 0 \\ 0 & 0 \\ 0 & 0 \\ 142.454 & 0 \\ 0 & 142.454 \end{bmatrix},$$

and

$$\boldsymbol{B}_2 = \begin{bmatrix} 4.907 & 0 & 0 \\ 0 & -2.000 & 0 \\ 0 & 0 & 0.020 \\ 0 & 195.861 & 0 \\ 0 & 0 & -1.959 \end{bmatrix}.$$

The associated inverter with the proposed speed estimator incorporated into the controller architecture is shown in Figure 4. The controller determines, for a given desired torque, the required inverter current, $\boldsymbol{i}^{e*}_{dqi} = \begin{bmatrix} i^{e*}_{di} & i^{e*}_{qi} \end{bmatrix}^T$, in the synchronous reference frame and the required slip frequency, ω^*_s. The controller will be described in greater detail in the following section. Other variables that appear in Figure 4 include the measured a- and b-phase inverter currents, $\breve{i}_{ai}$ and $\breve{i}_{bi}$, two measured line-to-line inverter voltages, u_{abi} and u_{bci}, the electrical frequency ω_e (which is integrated to determine the position of the synchronous reference frame θ_e), the vector of inverter phase current $\boldsymbol{i}^*_{abci} = \begin{bmatrix} i^*_{ai} & i^*_{bi} & i^*_{ci} \end{bmatrix}^T$ and the vector of switch commands $\boldsymbol{s}^*_{abc} = \begin{bmatrix} s^*_a & s^*_b & s^*_c \end{bmatrix}^T$. Setting s^*_x high indicates the upper transistor of x-phase should be turned on (and the lower transistor off), where 'x' may be 'a', 'b', or 'c'. The vector of stator voltages in the stationary frame, $\boldsymbol{u}_1$, is obtained from the measured line-to-line inverter voltages, u_{abi} and u_{bci}, employing first the $\boldsymbol{K}^s_{s,v}$-transformation followed by the wye-delta conversion, where

$$\boldsymbol{K}^s_{s,v} = \frac{2}{3}\begin{bmatrix} 1 & -1/2 \\ 0 & -\sqrt{3}/2 \end{bmatrix}.$$

The SCR block designates a synchronous current regulator, whose implementation is shown in Figure 5. This implementation comes from [13]. The currents $\breve{i}_{ai}$ and $\breve{i}_{bi}$ are transformed into the synchronous reference frame using the transformation

$$\boldsymbol{K}^e_{s,i} = \frac{2}{\sqrt{3}}\begin{bmatrix} \sin(\theta_e - \pi/6) & -\cos(\theta_e) \\ \cos(\theta_e - \pi/6) & \sin(\theta_e) \end{bmatrix}.$$

The transformed currents are then used to generate the error between the actual and the controller requested d- and q-axis currents. This error is multiplied by the integral gain $\left(\frac{1}{\tau_{scr}}\right)$, then integrated with the integration limits $\pm i_{fcl}$, and added back to $\boldsymbol{i}^{e*}_{dqi}$. The modified d- and q-axis current requests are transferred back to the abc variables using the inverse transformation $\boldsymbol{K}^{e^{-1}}_s|_{ltc}$, which consists of the first two columns of

$$\boldsymbol{K}^{e^{-1}}_s = \begin{bmatrix} \sin(\theta_e) & \cos(\theta_e) & 1 \\ \sin(\theta_e - \frac{2\pi}{3}) & \cos(\theta_e - \frac{2\pi}{3}) & 1 \\ \sin(\theta_e + \frac{2\pi}{3}) & \cos(\theta_e + \frac{2\pi}{3}) & 1 \end{bmatrix}.$$

A delta modulator is used to generate the switching commands, s_{abc}, for switching devices of the inverter $T_1, \ldots, T_6$. Every T_{sw} seconds, the modulator calculates the phase current error between i_{xi^*} from the SCR and $\breve{i}_{xi}$ as

$$e_{xi} = i^*_{xi} - \breve{i}_{xi}, \tag{16}$$

where 'x' may be 'a', 'b', or 'c'. Based on the sign of error in each phase in (16), switching command s^*_x is determined by

$$s^*_x = \begin{cases} 1 & \text{if } e_{xi} > 0 \\ 0 & \text{if } e_{xi} < 0. \end{cases} \tag{17}$$

The switching of the three phases is evenly staggered in time. For our study, T_{sw} is 100 μs.

VIII. DESCRIPTION OF THE CONTROL STRATEGY

In our simulations and lab experiments, we used an alternative q-d induction machine model (AQDM) using the maximum torque per amp (MTPA) control strategy recently proposed by Kwon and Sudhoff [14], [15]. We use the MTPA control strategy to validate the performance of the proposed speed estimator by using the estimated speed generated by the proposed speed estimator instead of the speed obtained from the mechanical speed sensor. In this section, we briefly review this AQMD based MTPA control strategy.

This control strategy was designed such that even induction machines that are driven at light or moderate loads for significant portions of their service life would operate with high efficiency. It is simple in structure and accounts for the effects of magnetizing and leakage saturation. The objective of this control strategy is to produce a desired torque with the minimum current that is favorable in terms of inverter losses and nearly optimal in terms of efficiency [16, Chapter 14]. In this control strategy, the root-mean-square magnitude of the stator current I_s and the slip frequency ω_s are expressed as functions of the desired torque, T^*_e. Kwon and Sudhoff [14], [15] has experimentally demonstrated that for the entire torque range, the proposed control strategy can find a slip frequency at which the produced torque is optimal for a given stator current (the maximum torque per amp condition) and is close to the desired torque. The steady-state equivalent circuit corresponding to the AQDM that was proposed in [14], [15]

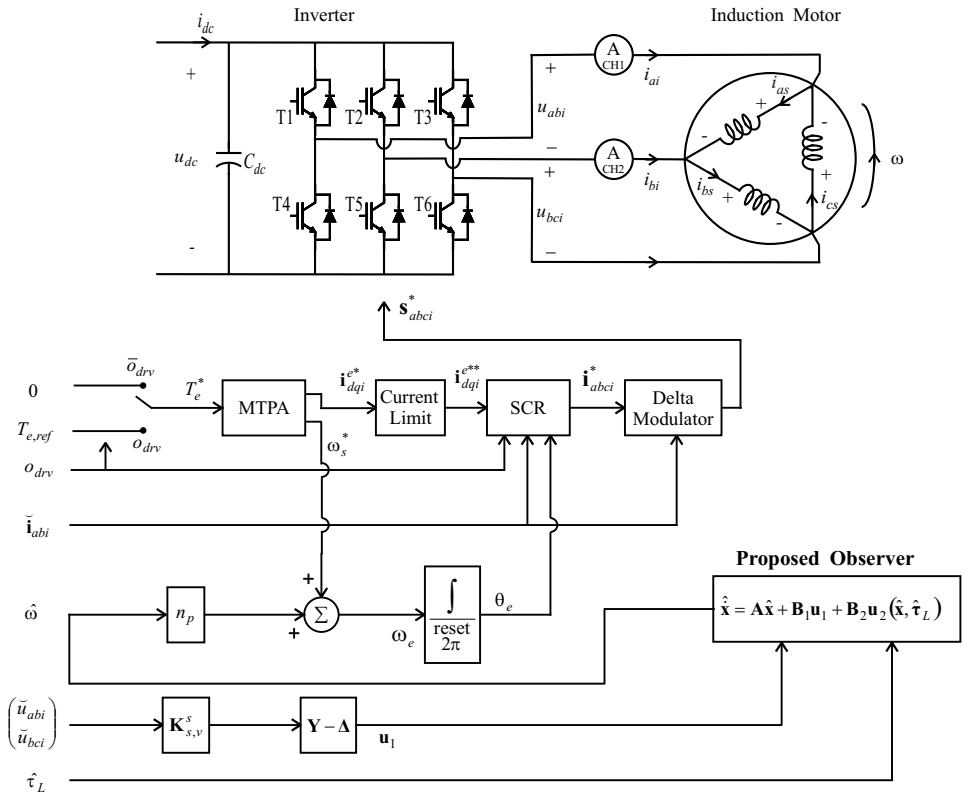

Fig. 4. Block diagram of current-controlled induction motor drive with the proposed speed observer incorporated into the controller architecture.

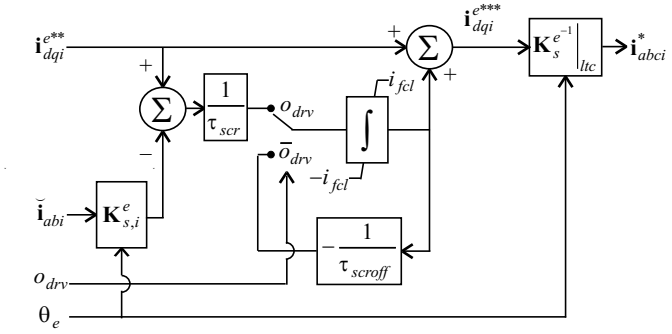

Fig. 5. Schematic diagram of the SCR.

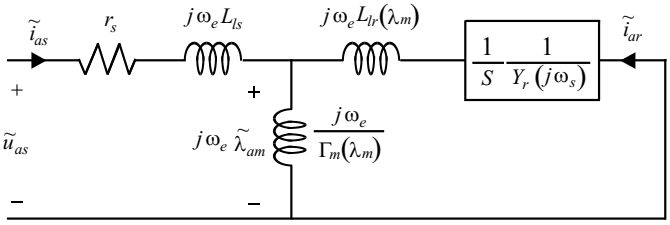

Fig. 6. Steady-state equivalent circuit of AQDM.

TABLE V
RESULTANT AQDM PARAMETERS.

$L_{ls}(\cdot)$		$\Gamma_m(\cdot)$		$Y_r(\cdot)$	
l_{s1}	9.06e-4	m_1	6.79e0	y_{a_1}	5.65e0
$L_{lr}(\cdot)$		m_2	6.62e-1	y_{τ_1}	3.21e-2
l_{r1}	1.40e-4	m_3	5.03e0	y_{a_2}	4.40e-2
l_{r2}	4.15e-3	m_4	1.85e0	y_{τ_2}	4.78e-4
l_{r3}	7.35e-1	m_5	8.68e-1	y_{a_3}	3.17e-3
l_{r4}	2.59e0	m_6	1.29e-1	y_{τ_3}	8.76e-8

is depicted in Figure 6. We use the following definitions: $\omega_s = \omega_e - n_p\omega$ and $\lambda_m = \sqrt{2}\left|\tilde{\lambda}_{am}\right|$. The slip S is defined as

$$S = \frac{\omega_e - n_p\omega}{\omega_e}.$$

The parameters in this equivalent circuit are:

$$\begin{aligned}
L_{ls} &= l_{s1}\,(\text{which is a constant}) \\
L_{lr}(\lambda_m) &= l_{r1} + \frac{l_{r2}}{1 + l_{r3}\lambda_m{}^{l_{r4}}} \\
\Gamma_m(\lambda_m) &= m_1 - m_2\lambda_m + e^{m_3(\lambda_m - m_4)} + e^{m_5(\lambda_m - m_6)} \\
Y_r(s) &= \frac{y_{a1}}{y_{\tau_1}s + 1} + \frac{y_{a2}}{y_{\tau_2}s + 1} + \frac{y_{a3}}{y_{\tau_3}s + 1},
\end{aligned}$$

where s denotes the differentiation operator in the Laplace domain. The AQDM parameters of the test induction motor were obtained using the method proposed in [14], [17]. The resultant motor parameters of the AQDM for this test motor are listed in Table V. Using the AQDM parameters given in Table V, an MTPA control strategy can now be derived. First note that the electromagnetic torque in the synchronous

reference frame may be written as

$$T_e = \frac{3}{2} n_p \left(\lambda^e_{qm} i^e_{ds} - \lambda^e_{dm} i^e_{qs} \right). \tag{18}$$

It is convenient to express (18) in terms of the slip frequency and the rms magnitude of the applied stator current. The relationship between the d-axis stator current in phasor representation and the d- and q-axis currents in the synchronous reference frame is

$$\sqrt{2}\tilde{i}_{ds} = i^e_{ds} - j i^e_{qs}. \tag{19}$$

Without loss of generality, we select the phase reference such that all the current is in the d-axis and reduce (19) to

$$\sqrt{2} I_s = i^e_{ds}, \tag{20}$$

where I_s is the magnitude of $\tilde{i}_{ds}$ which has only one component. Similarly, the relationship of magnetizing flux linkages may be expressed as

$$\sqrt{2}\tilde{\lambda}_{dm} = \lambda^e_{dm} - j\lambda^e_{qm}. \tag{21}$$

After algebraic manipulations of (18) and (21), we rewrite the electromagnetic torque in terms of the stator current and magnetizing flux linkage phasors as

$$T_e = 3 n_p \Im\left(\overline{\tilde{\lambda}_{dm}} I_s \right), \tag{22}$$

where $\Im(\cdot)$ denotes the operation of taking the imaginary part of the expression in the parentheses and the bar indicates the operation of complex conjugation. Using the AQDM steady-state equivalent circuit of Figure 6, we express $\tilde{\lambda}_{dm}$ as

$$\tilde{\lambda}_{dm}\left(\omega_s, I_s\right) = \frac{Z_{ag}\left(\lambda_m, \omega_s\right)}{j\omega_e} I_s, \tag{23}$$

where

$$Z_{ag}\left(\lambda_m, \omega_s\right) = \frac{\omega_e}{-j\Gamma_m\left(\lambda_m\right) + \frac{\omega_s}{j\omega_s L_{lr}(\lambda_m) + \frac{1}{Y_r(j\omega_s)}}} \tag{24}$$

and the subscript 'ag' in Z_{ag} indicates the impedance looking into the air-gap of the induction machine. The electromagnetic torque can now be expressed in terms of only ω_s and I_s. Substituting (23) into (22) yields

$$T_e\left(\omega_s, I_s\right) = 3 n_p \Im\left(\overline{\left(\frac{Z_{ag}\left(\lambda_m, \omega_s\right)}{j\omega_e} I_s \right)} I_s \right). \tag{25}$$

Note that the ω_e appearing in Z_{ag} in (24) cancels out the ω_e in the denominator of (25), and so $T_e\left(\omega_s, I_s\right)$ is independent of ω_e. Next, we note that $\lambda_m = \lambda_m\left(\omega_s, I_s\right)$ that appears in (25) satisfies the condition $\lambda_m = \sqrt{2}\left|\tilde{\lambda}_{dm}\right|$ and can be calculated by solving the nonlinear algebraic equation

$$\left|\omega_e \lambda_m\right| = \sqrt{2}\left|I_s Z_{ag}\left(\lambda_m, \omega_s\right)\right| \tag{26}$$

using, for example, the Newton-Raphson method for a given ω_s and I_s. We can now present a procedure for constructing an MTPA control strategy using (25). First, a set of stator current commands for I_s is be selected from nearly 0 A to somewhat over the rated current. The k-th point is denoted $I_{s,k}$. The optimum slip frequency for each current is identified by numerically maximizing (25) with $I_s = I_{s,k}$. The resulting value of the slip frequency is denoted $\omega_{s,k}$ and the corresponding value of the torque is denoted $T_{e,k}$. These data points are shown in Figure 7. Next, these data points are used

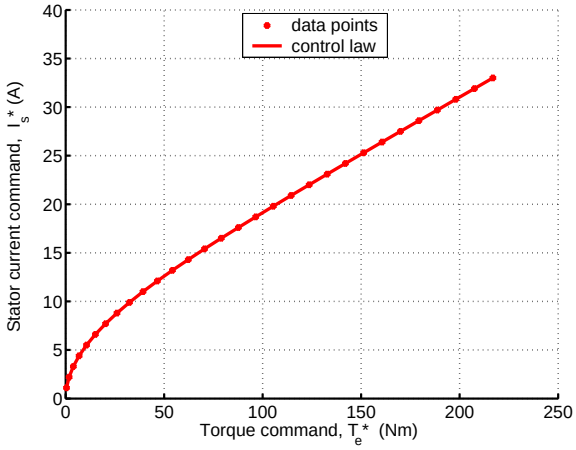

(a) Stator current command versus torque command.

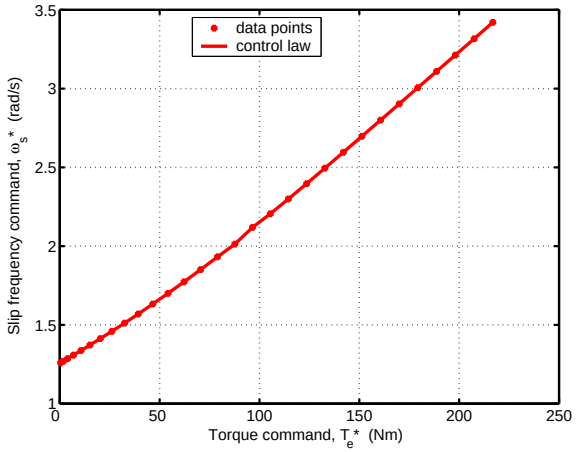

(b) Slip frequency command versus torque command.

Fig. 7. MTPA control law based on AQDM.

to construct a stator current and slip frequency control law. The data points $\{I_{s,k}, T_{e,k}\}$ are used to formulate a stator current control law of the form

$$I^*_s = a_1 T^*_e + a_2 T^{*b_1}_e + a_3 T^{*b_2}_e, \tag{27}$$

where a_1, a_2, a_3, b_1, and b_2 are selected by maximizing the objective fitness function defined by

$$f_{MTPA} = \frac{1}{\epsilon + \sqrt{\frac{1}{N_K}\sum_{k=1}^{N_K}\left|I_{s,k} - I^*_{s,k}\right|}}, \tag{28}$$

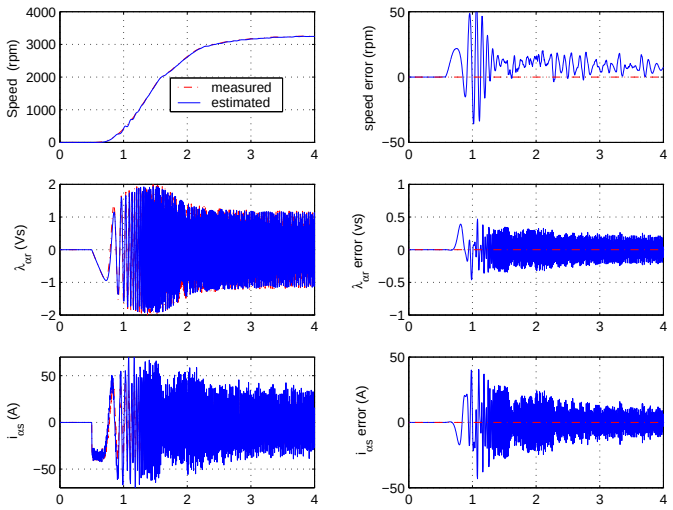

Fig. 8. Summary of a performance study of the proposed observer for zero initial conditions for the observer and the motor model.

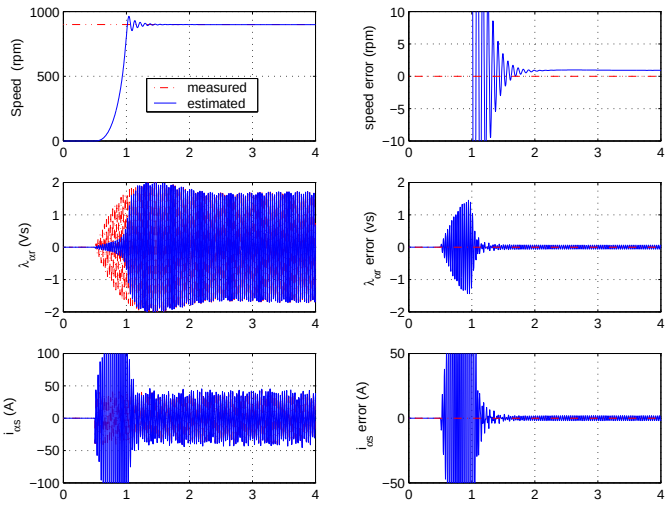

Fig. 9. Summary of a performance study of the proposed estimator for different initial conditions for the motor and the observer.

where ϵ is a small number $\left(10^{-3}\right)$ that is added to the denominator in order to prevent singularities in the unlikely event of a perfect fit, N_K is the size of a set of stator current commands, and $I^*_{s,k}$ is given by (27) with $T^*_e = T_{e,k}$.

Similarly, the data points $\{\omega_{s,k}, T_{e,k}\}$ are used to formulate a slip frequency control law of the form

$$\omega^*_s = c_0 + c_1 T^*_e + c_2 T^{*2}_e + c_3 T^{*3}_e + c_4 T^{*4}_e, \qquad (29)$$

where c_0, c_1, c_2, c_3, and c_4 are also chosen by maximizing (28) with I_s replaced with ω_s. We obtain $\omega^*_{s,k}$ from (29) with $T^*_e = T_{e,k}$. Together, (27) and (29) form the MTPA control strategy. Applying the above procedure to the test induction motor whose AQDM parameters are given in Table V, the formulas given by (27) and (29) become

$$I^*_s\left(T^*_e\right) = 0.109 T^*_e - 17.0 T^{*0.0177}_e + 18.5 T^{*0.0799}_e \qquad (30)$$

and

$$\begin{aligned} \omega^*_s\left(T^*_e\right) \quad = \quad & 1.4 - 2.4 \times 10^{-3} T^*_e + 176 \times 10^{-6} T^{*2}_e \\ & -933 \times 10^{-9} T^{*3}_e + 1.74 \times 10^{-9} T^{*4}_e. \end{aligned} \qquad (31)$$

The final analytically obtained values of the resulting MTPA control law based on the AQDM are also depicted in Figure 7.

IX. Simulation Studies

We performed computer simulations of the induction motor drive using the Advanced Continuous Simulation Language (ACSL) [18]. We note that the variables related to the MTPA control strategy were transformed into the synchronous reference frame while the variables used in the proposed estimator were transformed into the stationary reference frame. The first simulation study focused on the performance of the proposed speed estimator in an application where the characteristic of the load torque is known to have a form where the load torque is proportional to the mechanical rotor speed. In the study, the desired torque to the MTPA control strategy is set at 150 Nm and the estimated load torque employed by the proposed observer is proportional to the estimated rotor speed. Both initial conditions of the plant and the proposed estimator are set to zero. The results of this study are summarized in Figure 8. As can be seen in the figure, the proposed estimator predicts the rotor speed with good accuracy during the transient period as well as in the steady state period. Approximately 10% speed error is observed one second into the simulation, which then decreases. There is also some deviation in the stator current. This needs to be further investigated in future research.

The objective of the second study was the performance of the proposed estimator in an application where the characteristic of the load torque is unknown. We assumed that the transient response of the induction motor was short enough so that the load torque was equal to the the estimated electromagnetic torque. This enabled us to make use of the same equation as the estimated electromagnetic torque using the measured stator currents. Note that the measured stator currents are present in $\hat{\tau}_L$. In the experiment the test induction motor was driven to 900 rpm by the dynamometer and controlled in the torque mode with the desired torque of 150 Nm by the MTPA control strategy. The results of this simulation study are collected Figure 9, which shows that even though there are big deviations in the transient periods due to different initial conditions, the proposed estimator starts to track the actual speed closely in under 2 seconds.

X. Experimental Studies

In order to see if the results of computer simulations, described in the previous section, would predict the functioning of the proposed observer in real applications, its performance was investigated in a laboratory experiment, where the estimated load torque is unknown. The estimated load torque used by the proposed observer was obtained using the electromagnetic torque equation employing the measured stator currents. Therein, the test induction motor was driven

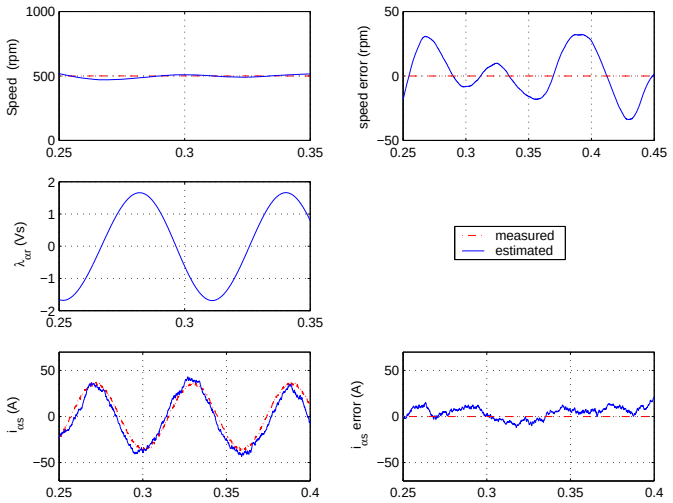

Fig. 10. Plots of the motor and the observer state variables in the steady state in an experimental performance study of the proposed observer.

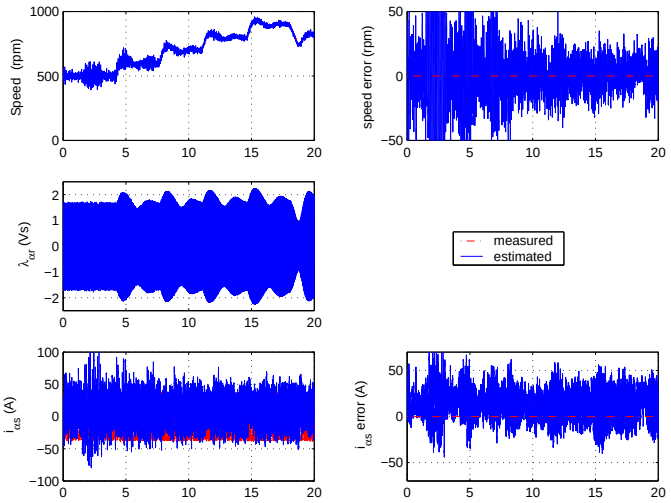

Fig. 11. Performance study of the proposed observer when rotor speed varies from 500 rpm to 900 rpm.

to 900 rpm with the torque command of 150 Nm using the MTPA control strategy. The results are shown in Figure 10. The experiment shows that the measured and estimated speeds are in good agreement during the steady-state period. The maximum speed estimation error is around 2.5%. We conclude that the proposed observer works well using stator voltages and measured stator currents in the estimated load torque in the steady state, that is, when the electromagnetic and load torques are equal. The second study was performed to investigate the tracking capability of the proposed estimator during the transient period with the same conditions as in the first experiment except that the rotor speed was varied arbitrarily in the range of 500 rpm to 900 rpm. As can be seen in Figure 11, the estimated speed follows the measured speed very closely during the steady state response, and even during the transient response. However, there are some deviations of the estimated stator currents from the measured currents. Further study is required to improve the proposed observer architecture in order to reduce the estimation error. Next, the application of the proposed estimator to speed sensorless induction machine drive was considered. We incorporated the proposed estimator into the MTPA control strategy based induction machine drive as shown in Figure 4, where we replaced the actual rotor speed, ω, by its estimated value, $\hat{\omega}$, produced by the proposed estimator. This laboratory experiment was conducted with the test induction motor driven at a speed of 900 rpm at a desired torque of 150 Nm. The electromagnetic torque measured at the estimated optimal slip frequency command ω_s^* defined in (31) was compared with the two sets of torque measurements taken at 0.9 and 1.1 times the slip frequency command ω_s^* in (31). These results are compared with the results of the MTPA control strategy based induction machine drive that uses the measured rotor speed and are shown in Figure 12. In both cases, the torque measured at the estimated optimal slip frequency command ω_s^* in (31) is larger than the torque produced at any other slip frequency indicating that

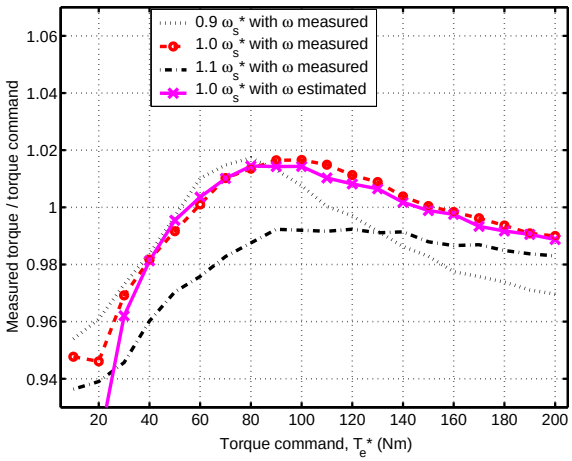

Fig. 12. Performance comparison study of the MTPA control strategy when the rotor speed is estimated by the proposed observer incorporated into the controller and when the rotor speed is measured by an encoder.

the estimated speed is accurate enough to substitute for the mechanical rotor speed sensor in this application. Note that the performance of the MTPA control strategy with the proposed estimator incorporated into the controller turns out to be poor because the speed estimation error is relatively large compared with the slip frequency command despite that the error is less than 1% at very light loads. Further studies on improving the observer performance at light loads is desired.

XI. Conclusions

In this paper, we investigated the use of observers in the sensorless control of induction motor drives. The three recently proposed rotor flux and speed observers [1], [3], [4] employed the fourth-order induction motor model assuming constant rotor speed and utilizing the measured stator currents. These observers perform well in the steady state or when the speed does not change aggressively. In the papers mentioned above, the performance of the proposed observers when the rotor

speed changes aggressively was not investigated. This aspect motivated us to employ the fifth-order induction motor model to propose an alternative rotor flux and speed observer. Simulation and laboratory experimental studies demonstrate that the proposed rotor flux and speed observer could do an excellent job in predicting the speed during the transient and steady state periods, even when applied in the sensorless control of the induction motor drives. However, further analysis should be performed to investigate the deviations of the estimated stator current from measured current when rotor speed changes aggressively, for example, from 500 rpm to 900 rpm.

ACKNOWLEDGMENT

This work was supported in part by ONR Grant N00014-02-1-0990 "Polytopic Modeling Based Stability Analysis and Genetic Optimization of Electric Warship Power System," by NAVSEA Contract N00024-2-NR-60427 "Naval Combat Survivability," and by ONR Grant N00014-02-1-0623 "National Naval Responsibility for Naval Engineering Education and Research for the Electric Naval Engineer."

REFERENCES

[1] H. Kubota, K. Matsuse, and T. Nakano, "DSP-based speed adaptive flux observer of induction motor," *IEEE Transactions on Industry Applications*, vol. 29, no. 2, pp. 344–348, March/April 1993.

[2] B. Ufnalski, "An application of neural networks to estimate rotor speed and stator flux in the cage induction motor drive system," Ph.D. dissertation, Institute of Control and Industrial Electronics, Warsaw University of Technology, Poland, 2004.

[3] A. Derdiyok, M. K. Güven, H. Rehman, N. Inanc, and L. Xu, "Design and implementation of a new sliding-mode observer for speed-sensorless control of induction machine," *IEEE Transactions on Industrial Electronics*, vol. 49, no. 5, pp. 1177–1182, October 2002.

[4] V. Utkin, J. Guldner, and J. Shi, *Sliding Mode Control in Electromechanical Systems*. London: Taylor & Francis, 1999.

[5] G. C. Verghese and S. R. Sanders, "Observers for flux estimation in induction machines," *IEEE Transactions on Industrial Electronics*, vol. 35, no. 1, pp. 85–94, February 1988.

[6] K. Rajashekara, A. Kawamura, and K. Matsuse, Eds., *Sensorless Control of AC Motor Drives: Speed and Position Sensorless Operation*. Piscataway, NJ 08855-1331: IEEE Press, 1996.

[7] F. E. Thau, "Observing the state of non-linear dynamic systems," *Int. J. Control*, vol. 17, no. 3, pp. 471–479, 1973.

[8] B. L. Walcott, M. J. Corless, and S. H. Żak, "Comparative study of non-linear state-observation techniques," *Int. J. Control*, vol. 45, no. 6, pp. 2109–2132, 1987.

[9] S. H. Żak and B. L. Walcott, "State observation of nonlinear control systems via the method of Lyapunov," in *Deterministic Control of Uncertain Systems*, A. S. I. Zinober, Ed. London, UK: Peter Peregrinus Ltd., 1990, ch. 16, pp. 333–350.

[10] S. R. Kou, D. L. Elliott, and T. J. Tarn, "Exponential observers for nonlinear dynamic systems," *Information and Control*, vol. 29, no. 3, pp. 204–216, November 1975.

[11] S. H. Żak, "On the stabilization and observation of nonlinear/uncertain dynamic systems," *IEEE Transactions on Automatic Control*, vol. 35, no. 5, pp. 604–607, May 1990.

[12] ——, "Authors's reply to the comments on "On the stabilization and observation of nonlinear/uncertain dynamic systems"," *IEEE Transactions on Automatic Control*, vol. 36, no. 11, pp. 1342–1343, November 1991.

[13] T. M. Rowan and R. J. Kerkman, "A new synchronous current regulator and an analysis of current-regulated PWM inverters," *IEEE Transactions on Industry Applications*, vol. 22, no. 4, pp. 678–690, July/August 1986.

[14] C. Kwon and S. D. Sudhoff, "A genetic algorithm based induction machine characterization procedure with application to maximum torque per amp control," 2004, submitted to IEEE Transactions on Energy Conversion.

[15] ——, "An improved maximum torque per amp control for induction machine drives," in *Proceedings of the 20th Annual IEEE Applied Power Electronics Conference and Exposition*, Austin,TX, March 2005, pp. 740–745.

[16] P. C. Krause, O. Wasynczuk, and S. D. Sudhoff, *Analysis of Electric Machinery and Drive Systems*, 2nd ed. Piscataway, NJ 08855-1331: IEEE Press and Wiley-Interscience, John Wiley & Sons, Inc., 2002.

[17] C. Kwon and S. D. Sudhoff, "A genetic algorithm based induction machine characterization procedure," in *Proceedings of the 2005 International Electric Machines and Drives Conference*, San Antonio,TX, May 2005, pp. 1358–1364.

[18] *Advanced Continuous Simulation Language (ACSL) Reference Manual*, AEgis Simulation, Inc., Huntsville, AL 35806, 1999.